Title

A PET/MRI study towards finding the optimal [^{18}F]Fluciclovine PET protocol for detection and characterisation of primary prostate cancer

Authors and affiliations

Mattijs Elschot[1], Kirsten M. Selnæs[1,2], Elise Sandsmark[1], Brage Krüger-Stokke[1,3], Øystein Størkersen[4], May-Britt Tessem[1], Siver A. Moestue[1,5], Helena Bertilsson[6,7], Tone F. Bathen[1,2]

[1]Dept. Circulation and Medical Imaging, NTNU, Norwegian University of Science and Technology, Trondheim, Norway

[2]St. Olavs Hospital, Trondheim University Hospital, Trondheim, Norway

[3]Dept. Radiology, St. Olavs Hospital, Trondheim University Hospital, Trondheim, Norway

[4]Dept. Pathology, St. Olavs Hospital, Trondheim University Hospital, Trondheim, Norway

[5]Dept. Laboratory Medicine, Children's and Women's Health, NTNU, Norwegian University of Science and Technology, Trondheim, Norway

[6]Dept. Urology, St. Olavs Hospital, Trondheim University Hospital, Trondheim, Norway

[7]Dept. Cancer Research and Molecular Medicine, NTNU, Norwegian University of Science and Technology, Trondheim, Norway

Corresponding author

Mattijs Elschot

Mail MTFS*3.1313

POBox 8905

N-7491 Trondheim

T +4773598634

F +31887555491

mattijs.elschot@ntnu.no

Keywords

[^{18}F]Fluciclovine, [^{18}F]FACBC, Prostate Cancer, PET/MRI, Dynamic PET

Acknowledgements

The authors acknowledge Professor Frode Willoch, Institute of Basic Medical Sciences, University of Oslo, for his support with [^{18}F]Fluciclovine PET imaging.

Abstract

Purpose [^{18}F]Fluciclovine PET imaging shows promise for the assessment of prostate cancer. The purpose of this PET/MRI study is to optimise the PET imaging protocol for detection and characterisation of primary prostate cancer, by quantitative evaluation of the dynamic uptake of [^{18}F]Fluciclovine in cancerous and benign tissue.

Methods Patients diagnosed with high-risk primary prostate cancer underwent an integrated [^{18}F]Fluciclovine PET/MRI exam before robot-assisted radical prostatectomy with extended pelvic lymph node dissection. Volumes-of-interest (VOIs) of selected organs (prostate, bladder, blood pool) and sub-glandular prostate structures (tumour, benign prostatic hyperplasia (BPH), inflammation, healthy tissue) were delineated on T2-weighted MR images, using whole-mount histology samples as a reference. Three candidate windows for optimal PET imaging were identified based on the dynamic curves of the mean and maximum standardised uptake value (SUV_{mean} and SUV_{max}, respectively). The statistical significance of differences in SUV between VOIs were analysed using Wilcoxon rank sum tests ($p<0.05$, adjusted for multiple testing).

Results Twenty-eight (28) patients (median (range) age: 66 (55-72) years) were included. An early (W1: 5-10 minutes post-injection) and two late candidate windows (W2: 18-23; W3: 33-38 minutes post-injection) were selected. Late compared with early imaging was better able to distinguish between malignant and benign tissue (W3, SUV_{mean}: tumour vs BPH 2.5 vs 2.0 ($p<0.001$), tumour vs inflammation 2.5 vs 1.7 ($p<0.001$), tumour vs healthy tissue 2.5 vs 2.0 ($p<0.001$); W1, SUV_{mean}:

tumour vs BPH 3.1 vs 3.1 (p=0.771), tumour vs inflammation 3.1 vs 2.2 (p=0.021), tumour vs healthy tissue 3.1 vs 2.5 (p<0.001)) as well as between high-grade and low/intermediate-grade tumours (W3, SUV_{mean}: 2.6 vs 2.1 (p=0.040); W1, SUV_{mean}: 3.1 vs 2.8 (p=0.173)). These differences were relevant to the peripheral zone, but not the central gland.

Conclusion Late-window [^{18}F]Fluciclovine PET imaging shows promise for distinguishing between prostate tumours and benign tissue and for assessment of tumour aggressiveness.

Introduction

Prostate cancer (PCa) is the most frequently detected type of cancer in men in developed countries [1]. Patients may have an indolent type of PCa for which active surveillance suffices, or more aggressive PCa that requires active treatment [2]. Together with prostate-specific antigen (PSA) blood assays and prostate biopsy samples, medical imaging is increasingly being used for stratification of patients with indolent and clinically significant disease.

The combination of T2-weighted (T2W), diffusion-weighted (DWI), and dynamic contrast-enhanced (DCE) MRI, also known as multi-parametric MRI (mpMRI), has indisputable value for staging of the local tumour extent (T-staging) [2, 3]. However, the accuracy of mpMRI for detection of clinically significant disease is highly variable [4], while grading of tumour aggressiveness seems restricted by overlapping values between Gleason scores [5]. Furthermore, MRI lacks the sensitivity for accurate staging of the regional lymph nodes (N-staging) [6]. PET/CT imaging with the synthetic amino acid analog radiotracer anti-1-amino-3-[^{18}F]fluorocyclobutane-1-carboxylic acid ([^{18}F]Fluciclovine or [^{18}F]FACBC), on the other hand, shows promise for N-staging in both primary [7] and recurrent PCa [7-9] and may be complementary to mpMRI for detection and characterisation of prostate tumours [10, 11].

Motivated by these results, our group set out to investigate the merit of simultaneous [^{18}F]Fluciclovine PET/MRI for the assessment of primary PCa. In comparison to separate mpMRI and PET/CT, simultaneous PET/MRI has the advantage of reduced radiation exposure, shorter (cumulative) scan times, and intrinsic alignment of the PET and MR images. The ideal PET/MR imaging protocol should be as short as possible, while not compromising the image quality of either modality. For tracers with fast uptake kinetics like [^{18}F]Fluciclovine [11-13], however, careful timing of the PET acquisition window is required to optimise the available diagnostic information [10, 11]. For this purpose, there is need for better understanding of the dynamic uptake pattern in regions of cancerous and benign tissue.

The specific purpose of this study is to find the optimal timing of [^{18}F]Fluciclovine PET imaging for detection and characterisation of primary PCa, by quantitative assessment of the dynamic uptake in histologically verified prostate tumours, regions of benign prostatic hyperplasia (BPH) and inflammation, and the surrounding healthy tissue. The results extend the findings of earlier work investigating the uptake dynamics of [^{18}F]Fluciclovine [7, 10-13] and support the optimisation of clinical PET/MR and PET/CT imaging protocols for the assessment of primary PCa.

Materials and methods

Patients

High-risk patients (biopsy Gleason score ≥ 8 and/or prostate specific antigen (PSA) ≥ 20 and/or clinical stage ≥ cT3 (*2*)) scheduled for robot-assisted radical prostatectomy (RARP) with extended pelvic lymph node dissection (ePLND) were recruited for a prospective study investigating the merit of combined [^{18}F]Fluciclovine PET/MRI for loco-regional staging of primary PCa (ClinicalTrials.gov; identifier NCT02076503). The study was approved by our institution (St. Olavs Hospital, Trondheim University Hospital) and the Regional Committee for Medical and Health Research Ethics, Central Norway (identifier 2013/1513). All patients gave written informed consent before enrollment.

Imaging

Patients underwent a PET/MRI exam on a 3 T Biograph mMR scanner (Siemens Medical Systems, Erlangen, Germany) prior to surgery. [^{18}F]Fluciclovine was produced by the Norwegian Medical Cyclotron Centre in Oslo by methods previously described [13]. The PET/MRI protocol consisted of a full clinical mpMRI examination for T+N-staging, combined with 45 minutes of simultaneous PET imaging. Data acquisition was performed in two (largely overlapping) bed positions (Fig. 1, Table 1): bed position 1 (BP1) was positioned to have the prostate in the isocenter of the magnet and was used for the prostate-specific MR sequences and the last 20 minutes of list-mode PET imaging. Bed position 2 (BP2) was positioned to cover the lymph nodes from the pelvic floor up to the ureteral

crossing of the common iliac vessels and was used for the lymph node-specific MR sequences and the first 25 minutes of list-mode PET imaging. Importantly, the prostate gland was completely covered by both bed positions, thus providing a total of 45 minutes of sequential list-mode PET data for analysis of the tracer dynamics.

Surgery and histopathology

RARP with ePLND was performed according to EAU guidelines [2]. The removed tissue was fixed in 4% buffered formaldehyde before further histopathological analysis. The prostate gland was serially sectioned from apex to base in 4 mm thick slices perpendicular to the urethra. The most inferior slice (apex) and most superior slice (base) were additionally sectioned in longitudinal direction for optimal histopathological evaluation of extracapsular extension. All slices were embedded in paraffin before 3.5 µm thick sections were cut for staining with hematoxylin and eosin. A pathologist specialized in uropathology outlined cancer foci and regions of BPH and inflammation and described cancer grade according to the Gleason Scoring system [14].

Volumes-of-interest

Three-dimensional volumes-of-interest (VOIs) were delineated for several organs and sub-glandular prostate structures. At the organ level, the whole bladder and ten consecutive transverse slices of the external iliac arteries (blood pool) were delineated on T2SPACE images using 3D Slicer [15]. The whole prostate, including the complete apex and base, was delineated on transverse T2TSE images using OsiriX [16]. With regard to sub-glandular prostate structures, the whole-mount histology slides were ordered from apex to base and spatially matched to their corresponding transverse T2TSE slices based on visual comparison. Subsequently, tumours, inflammatory tissue, and regions of BPH were delineated on the T2TSE images while using histopathology as a reference. Sub-glandular structures in the inferior part of the apex and in the superior part of the base of the prostate could not be evaluated because the corresponding histology samples could not be reliably matched to the transverse T2TSE images due to their longitudinal slice direction. Healthy prostate tissue VOIs were

automatically obtained consisting of all voxels in the prostate (excluding inferior apex and superior base) that were not part of the tumour, inflammation, or BPH VOIs. Healthy VOIs were subsequently eroded to avoid potential partial volume effects resulting from the limited PET resolution and/or small registration errors. The volume (mL) and anatomical location (peripheral zone or central gland) were recorded for each of the sub-glandular VOIs. Tumours were assigned to be high-grade (primary Gleason ≥ 4 and/or any Gleason ≥ 5, i.e. ≥ Grade group 3 [17]) or low/intermediate-grade. Furthermore, each VOI was assigned a confidence score (1 not confident; 2 reasonably confident; 3 confident), which expressed how well the delineated VOI resembled the corresponding structure on histology. Sub-glandular VOIs with volume < 0.5 mL and/or confidence score < 2 were excluded from further analysis.

The MR images were co-registered to the PET images to transfer the VOIs and to account for small misalignments due to patient movement. A 3-level smoothing pyramid was used for multi-resolution rigid registration (Euler transform) based on mutual information (advanced Mattes mutual information) in Elastix, [18]. To guarantee a similar signal-to-noise ratio between the PET images of BP2 and BP1, it was checked that all VOIs were positioned well within both field-of-views after transformation.

Dynamic uptake curves and candidate windows

The PET list-mode data were binned into 20 time bins (4x15, 4x30, 4x60, 6x120 and 2x180 seconds) for BP2 and 4 time bins (4x300 seconds) for BP1, before reconstruction with manufacturer provided software (Siemens HDPET, 344 x 344 matrix, 3 iterations, 21 subsets, 4 mm FWHM Gaussian filter). For each of the VOIs, dynamic uptake curves were obtained by calculating the mean and maximum standardised uptake value (SUV_{mean} and SUV_{max}, respectively) as a function of time, using linear interpolation.

Three time windows of 5-minutes duration were identified as candidates for PET imaging based on the dynamic uptake curves. Subsequently, SUV_{mean} and SUV_{max} were calculated for each of these windows.

Statistical analysis

Descriptive statistics are presented as median and range. The statistical significance of differences in SUV_{mean} and SUV_{max} between prostate and bladder, prostate and blood pool, and tumour and all other sub-glandular VOIs were analysed for each time point on the dynamic uptake curves and for each of the candidate windows using Wilcoxon rank sum tests. For the candidate windows, statistical differences between high-grade and low/intermediate-grade tumours were investigated, and a separate analysis of the peripheral zone and central gland was performed. P-values < 0.05 after Benjamini-Hochberg adjustment for multiple testing [19] were considered statistically significant. Receiver operating characteristic (ROC) curve analysis was performed to evaluate the performance of SUV in distinguishing tumours from benign tissue, and high-grade tumours from all other tissue. Unless indicated otherwise, MATLAB version 8.5 (The MathWorks Inc., Natick, MA) was used for image processing and statistical analysis.

Results

Patients, surgery, and histopathology

Twenty-eight (28) patients of median (range) age 66 (55-72) years, height 181 (168-192) cm, and weight 83.5 (73-105) kg were included in the study. Median (range) PSA was 14.6 (3.7-56.9) ng/mL, median (range) biopsy Gleason score was 8 (7-9), and the clinical stage ranged from cT2b to cT3b. The median (range) time between PET/MR imaging and surgery was 8 (5–32) days. RARP and ePLND were successfully performed in 26 patients, whereas 2 patients received RARP without ePLND.

Imaging and volumes-of-interest

The median (range) activity administered to the patients was 327 (283-384) MBq. PET acquisition in BP2 and BP1 was started 1.0 (0.4–3.25) minutes and 27.6 (26.8–35.3) minutes post-injection, respectively. PET acquisition in BP1 was prematurely halted after 10 and 15 minutes in 3 and 2 patients, respectively.

In total, 28 prostate, 28 bladder, 28 blood pool, 39 tumour (14 low/intermediate-grade, 25 high-grade), 36 BPH, 6 inflammation, and 28 healthy VOIs were included for analysis.

Dynamic uptake curves

The dynamic SUV_{mean} curves and a corresponding graphical overview of the statistical differences in SUV_{mean} between VOIs are presented in Fig. 2. The dynamic SUV_{max} curves showed a similar pattern. Based on these results, 3 candidate time windows were identified; an early window (W1: 5-10 minutes post-injection (BP2)) was selected because of the high contrast between the prostate and the nearby bladder. Two late windows (W2: 18-23 minutes post-injection (BP2); W3: 33-38 minutes post-injection (BP1)) were identified as candidates for optimising contrast between prostate tumours and benign tissue.

Candidate windows

In all three candidate windows, both SUV_{mean} and SUV_{max} were significantly higher in the prostate than in the blood pool. Both SUV_{mean} and SUV_{max} were higher in the prostate than in the bladder in W1, but not in W2 and W3 (Table 2). The differences in SUV_{mean} and SUV_{max} between tumour and benign tissue (Table 3), as well as between high-grade and low/intermediate-grade tumours (Table 4), were generally most significant in W3. A similar trend was observed when only considering the peripheral zone, whereas between the central gland structures no significant differences were found. Fig. 3 clearly illustrates the effect of window timing on SUV contrast. ROC analysis (Fig. 4) gave the highest areas under the curves (AUC) in W3, both for distinguishing between tumours and benign tissue (AUC 80%; sensitivity 74%; specificity 71%) and for distinguishing between high-grade tumours

and all other tissue (AUC 85%; sensitivity 76%; specificity 82%). A complete overview of the ROC analysis results is provided as ESM 1.

Discussion

[^{18}F]Fluciclovine PET/CT was recently approved by the FDA for use in recurrent PCa and an increase in the use of this tracer for primary PCa may therefore also be anticipated. The aim of this PET/MRI study was to find the optimal timing of [^{18}F]Fluciclovine PET imaging for detection and characterisation of primary PCa, by quantitative assessment of the dynamic uptake in histologically verified cancerous and benign tissue. We found that late-window PET imaging (33–38 minutes post-injection) differentiated best between prostate tumours and benign tissue, as well as between high-grade and low/intermediate-grade tumours.

Although the dynamic uptake pattern of [^{18}F]Fluciclovine in primary PCa has been investigated before [7, 10-13], our study is the first to use integrated PET/MRI for this purpose. This approach has the advantage of intrinsically providing near-perfect co-alignment between the PET and the MR images, which enables accurate VOI delineation on MR images with excellent soft-tissue contrast. The resulting organ-based dynamic uptake patterns were found to be in good agreement with those reported previously [7, 11-13], most importantly showing fast uptake and slow wash-out in the prostate, low bladder uptake until approximately 10 minutes post-injection, and stable blood pool activity from approximately 5 minutes post-injection.

Our results indicate that a late-window [^{18}F]Fluciclovine PET imaging approach is optimal for detection and characterisation of primary prostate tumours and may partly ameliorate previously reported limitations with regard to distinguishing between benign and malignant prostate tissue [10, 11]. We found SUV_{mean} to be a more useful parameter than SUV_{max}, due to overlapping values in healthy tissue and tumours for the latter. The relatively high SUV_{max} in healthy tissue may be the result of its sensitivity to noise, small registration errors, and/or activity in the urethra. Overlap in

SUV between malignant and benign prostate lesions has been reported as a major source of false-positive findings [10, 11], which seriously threatens the applicability of [^{18}F]Fluciclovine PET/CT as a standalone modality. For example, Turkbey *et al.* did not find significant differences in SUV_{max} between tumours and regions of BPH using an imaging window of 15–20 minutes post-injection [11]. Schuster *et al* did find significant differences in SUV_{max} between malignant and benign tissue, but with considerable overlap [10]. They reported an optimal diagnostic accuracy of 71% based on visual analysis using a late imaging window (26–30 minutes post-injection). We found a similarly moderate accuracy (72%) for distinguishing tumours from benign tissue based on a SUV_{mean} threshold of 2.1. On a patient level, this would have translated in correctly detecting prostate tumours in 24 of the 28 patients (86%). However, to decrease the risk of overtreatment of indolent disease, some authors suggest that it would be beneficial to find tumours of clinical significance only [3], as these are associated with a poor prognosis [17]. Our results indicate that late-window [^{18}F]Fluciclovine PET imaging may have potential for this purpose, with a sensitivity and specificity of 76% and 82%, respectively, for distinguishing between high-grade tumours and all other tissue.

In general, the observed differences in SUV were significant but small, which may hamper clinical decision making based on [^{18}F]Fluciclovine PET images alone. Nevertheless, it seems like [^{18}F]Fluciclovine PET imaging is useful for the detection and characterization of lesions in the peripheral zone, whereas it should be used with caution in the central gland. For the latter, no significant differences in late-window SUV_{mean} and SUV_{max} were found between tumours and benign lesions and between tumours and healthy prostate tissue. On the other hand, late-window [^{18}F]Fluciclovine PET imaging did seem to enable a good separation between high-grade central gland tumours and all other central gland tissue (Figure 4). However, only six central gland tumours were available for analysis in this cohort, so these results will need to be verified. Future research will also be directed towards investigating if the combination of late-window SUV and mpMRI-derived parameters, rather than parameters from either modality alone, can support radiological reading.

This study has limitations. First, only high-risk patients were included, as part of an overarching study to determine the diagnostic performance of combined [^{18}F]Fluciclovine PET/MRI for T+N-staging of primary PCa. Although this pre-selected patient cohort gave us the opportunity to investigate the dynamic uptake of [^{18}F]Fluciclovine in cancerous and benign tissue with spatially matched histology as a reference, it also imposed restrictions on the interpretation of the results for prostate cancer in general, especially with regard to separating high-grade tumours from low/intermediate-grade tumours. Consequently, we stress that our results should be verified with independent datasets before generalisation to patients with low and intermediate-risk PCa is justified. A second limitation is the retrospective nature of this quantitative analysis; the VOIs were identified on the MR images using the histology slides as a reference, which could lead to different results in comparison with reading of the PET images blinded to histology, as would be the case in clinical practice. As a third limitation, the inferior part of the apex and the superior part of the base of the prostate had to be excluded from the sub-glandular analysis. The corresponding histology slides were sectioned in a longitudinal direction and could therefore not be reliably used as a reference for delineation of the VOIs on the transverse MR images. In practice, this meant that a median (range) of 17% (3 – 30%) of the prostate volume was excluded from quantitative analysis. Although histopathology revealed that cancer was present in these structures in 23/28 patients, only two independent tumour foci could be identified that were most likely not part of a larger mid-gland tumour extending into the apex and/or base of the prostate. We therefore estimate that excluding the inferior apex and superior base of the prostate had only a small effect on the outcome of the study. For whole-prostate analysis on the organ level, the complete apex and base were included in the VOI.

This work is focused on optimising the [^{18}F]Fluciclovine PET imaging protocol for detection and characterisation of prostate tumours. N-staging before RARP with ePLND is, however, another interesting application of [^{18}F]Fluciclovine PET, which would ideally be performed in the same examination. The uptake patterns described in the scarce amount of evidence that is currently available on this subject show immediate [^{18}F]Fluciclovine uptake and relatively fast wash-out in the

lymph nodes [7, 13]. Accordingly, we found a trend of higher tracer uptake in the early time-window than in the late time-windows using a preliminary analysis of four lymph node metastases that were clearly visible on the PET images (ESM 2). We therefore speculate that a dual-window PET protocol that combines early-window with late-window imaging might be optimal for detection and characterisation of both prostate tumours and lymph node metastases. However, this needs further investigation and optimising the PET protocol for imaging of lymph node metastases is subject of future research.

The proposed late-window PET imaging protocol can easily be combined with standard clinical MR protocols for T-staging or T+N-staging on an integrated PET/MRI scanner. For example, for T+N-staging one could start with acquiring the MR images for lymph node evaluation, potentially simultaneously with early-window PET imaging [7, 13], immediately followed by simultaneous late-window PET/MR imaging of the prostate. On a PET/CT scanner, late-window PET imaging could be implemented as a dedicated prostate examination or in combination with a whole-body examination for N-staging. In both cases, however, an additional mpMRI examination would still be required for T-staging [2]. In this work, we have used the MR images for delineation of the VOIs only, as the sole purpose was to find the optimal timing of the PET acquisition. In future work, however, we will investigate the diagnostic performance of combined [^{18}F]Fluciclovine PET/mpMRI for detection, grading, and loco-regional staging of primary PCa in clinical practice. To this effect, the results from the quantitative analysis presented here will form a solid basis for providing the nuclear medicine physicians and radiologists with the most powerful PET images.

Conclusion

Quantitative evaluation of the dynamic uptake of [^{18}F]Fluciclovine shows that a late-window PET imaging approach may be useful for distinguishing between prostate tumours and benign prostate tissue and for the assessment of prostate tumour aggressiveness. However, further studies are

warranted to evaluate the diagnostic performance of late-window [^{18}F]Fluciclovine PET in clinical practice, both as a stand-alone modality and in conjoint use with MRI.

Compliance with ethical standards

Funding This study was funded by The Norwegian Cancer Society (grant number 100792).

Conflicts of interest The authors declare that they have no conflicts of interest.

Ethical approval All procedures performed in studies in studies involving human participants were in accordance with the ethical standards of the institutional and/or national research committee and with the 1964 Helsinki declaration and its later amendments or comparable ethical standards.

Informed consent Informed consent was obtained from all individual participants included in the study.

References

1. Torre LA, Bray F, Siegel RL, Ferlay J, Lortet-Tieulent J, Jemal A. Global cancer statistics, 2012. CA Cancer J Clin. 2015;65:87-108.
2. Heidenreich A, Bastian PJ, Bellmunt J, Bolla M, Joniau S, van der Kwast T et al. EAU guidelines on prostate cancer. part 1: screening, diagnosis, and local treatment with curative intent-update 2013. Eur Urol. 2014;65:124-37.
3. Barentsz JO, Weinreb JC, Verma S, Thoeny HC, Tempany CM, Shtern F et al. Synopsis of the PI-RADS v2 Guidelines for Multiparametric Prostate Magnetic Resonance Imaging and Recommendations for Use. Eur Urol. 2016;69:41-9.
4. Futterer JJ, Briganti A, De Visschere P, Emberton M, Giannarini G, Kirkham A et al. Can Clinically Significant Prostate Cancer Be Detected with Multiparametric Magnetic Resonance Imaging? A Systematic Review of the Literature. Eur Urol. 2015;68:1045-53.
5. Kobus T, Vos PC, Hambrock T, De Rooij M, Hulsbergen-Van de Kaa CA, Barentsz JO et al. Prostate cancer aggressiveness: in vivo assessment of MR spectroscopy and diffusion-weighted imaging at 3 T. Radiology. 2012;265:457-67.
6. Hovels AM, Heesakkers RA, Adang EM, Jager GJ, Strum S, Hoogeveen YL et al. The diagnostic accuracy of CT and MRI in the staging of pelvic lymph nodes in patients with prostate cancer: a meta-analysis. Clin Radiol. 2008;63:387-95.
7. Schuster DM, Votaw JR, Nieh PT, Yu W, Nye JA, Master V et al. Initial experience with the radiotracer anti-1-amino-3-18F-fluorocyclobutane-1-carboxylic acid with PET/CT in prostate carcinoma. J Nucl Med. 2007;48:56-63.
8. Schuster DM, Nieh PT, Jani AB, Amzat R, Bowman FD, Halkar RK et al. Anti-3-[(18)F]FACBC positron emission tomography-computerized tomography and (111)In-capromab pendetide single photon

emission computerized tomography-computerized tomography for recurrent prostate carcinoma: results of a prospective clinical trial. J Urol. 2014;191:1446-53.
9. Nanni C, Zanoni L, Pultrone C, Schiavina R, Brunocilla E, Lodi F et al. F-FACBC (anti1-amino-3-F-fluorocyclobutane-1-carboxylic acid) versus C-choline PET/CT in prostate cancer relapse: results of a prospective trial. Eur J Nucl Med Mol Imaging. 2016.
10. Schuster DM, Taleghani PA, Nieh PT, Master VA, Amzat R, Savir-Baruch B et al. Characterization of primary prostate carcinoma by anti-1-amino-2-[(18)F] -fluorocyclobutane-1-carboxylic acid (anti-3-[(18)F] FACBC) uptake. Am J Nucl Med Mol Imaging. 2013;3:85-96.
11. Turkbey B, Mena E, Shih J, Pinto PA, Merino MJ, Lindenberg ML et al. Localized prostate cancer detection with 18F FACBC PET/CT: comparison with MR imaging and histopathologic analysis. Radiology. 2014;270:849-56.
12. Schuster DM, Nanni C, Fanti S, Oka S, Okudaira H, Inoue Y et al. Anti-1-amino-3-18F-fluorocyclobutane-1-carboxylic acid: physiologic uptake patterns, incidental findings, and variants that may simulate disease. J Nucl Med. 2014;55:1986-92.
13. Sorensen J, Owenius R, Lax M, Johansson S. Regional distribution and kinetics of [18F]fluciclovine (anti-[18F]FACBC), a tracer of amino acid transport, in subjects with primary prostate cancer. Eur J Nucl Med Mol Imaging. 2013;40:394-402.
14. Epstein JI. An update of the Gleason grading system. J Urol. 2010;183:433-40.
15. Fedorov A, Beichel R, Kalpathy-Cramer J, Finet J, Fillion-Robin JC, Pujol S et al. 3D Slicer as an image computing platform for the Quantitative Imaging Network. Magn Reson Imaging. 2012;30:1323-41.
16. Rosset A, Spadola L, Ratib O. OsiriX: an open-source software for navigating in multidimensional DICOM images. J Digit Imaging. 2004;17:205-16.
17. Epstein JI, Zelefsky MJ, Sjoberg DD, Nelson JB, Egevad L, Magi-Galluzzi C et al. A Contemporary Prostate Cancer Grading System: A Validated Alternative to the Gleason Score. Eur Urol. 2016;69:428-35.
18. Klein S, Staring M, Murphy K, Viergever MA, Pluim JP. elastix: a toolbox for intensity-based medical image registration. IEEE Trans Med Imaging. 2010;29:196-205.
19. Benjamini Y, Hochberg Y. Controlling the False Discovery Rate: A Practical and Powerful Approach to Multiple Testing. J R Stat Soc Series B Stat Methodol. 1995;57:289-300.

Figure captions

Fig. 1 An illustrative overview of the imaging protocol and the different bed positions (BP). BP1 is positioned to have the prostate (red oval) in the isocenter of the scanner. BP2 is positioned to cover the pelvic lymph nodes (blue ovals), as well as the prostate. After injection of [^{18}F]Fluciclovine, the first 25 minutes of PET imaging are performed in BP2 and the last 20 minutes in BP1

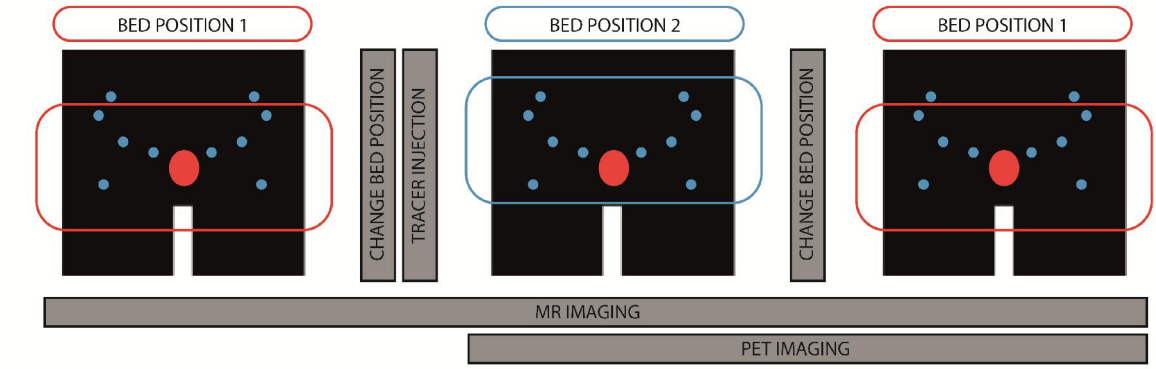

Fig. 2 Median (line + marker) and median absolute deviation (shaded area) of the dynamic SUV_{mean} curves in the organ VOIs (a) and the sub-glandular VOIs (b), together with a graphical illustration of the statistical test results for each time point on the dynamic SUV_{mean} curves, overlaid with the position of the early (W1) and late candidate windows (W2 and W3) (c). The median absolute deviation is calculated as the median value of the absolute differences between the individual SUVs and their median value

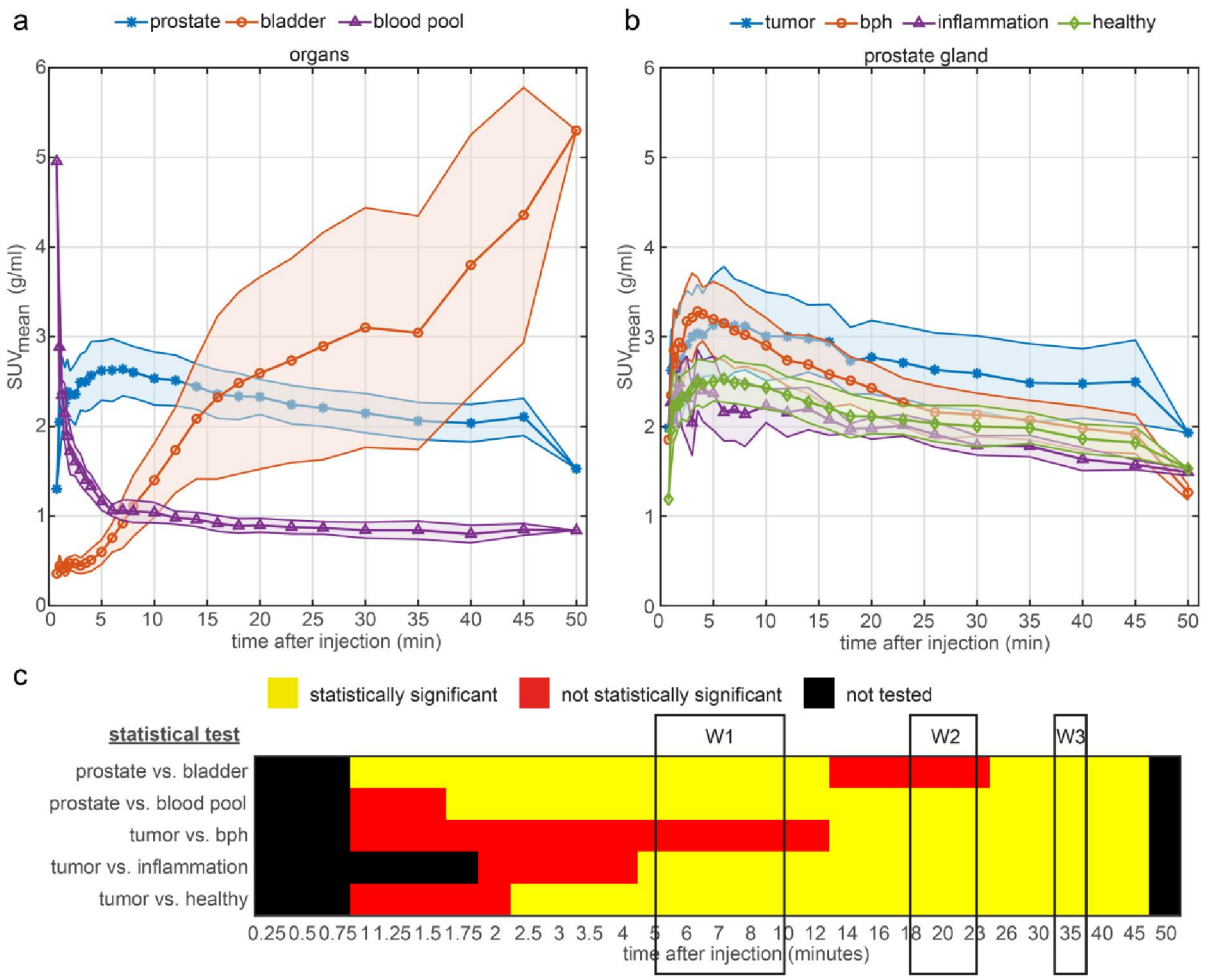

Fig. 3 T2-weighted TSE (a) and PET images from W1 (b), W2 (c), and W3 (d) overlaid with the contours of the prostate (light blue), regions of BPH (green) and tumours (blue). The insert in (a) shows the corresponding histology slide. The contrast in SUV between BPH and tumours was different in all windows. The smallest tumours were excluded from analysis (< 0.5 mL). All PET images were linearly scaled from 0–6 SUV

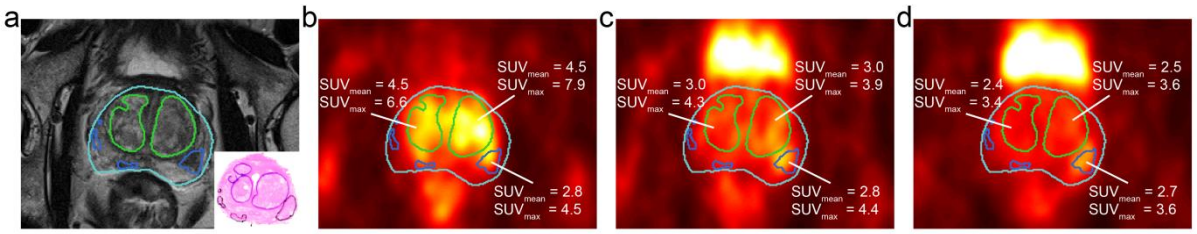

Fig. 4 ROC curves of the parameters (W3) best separating tumours from benign tissue (a) and high-grade tumours from all other tissue (b)

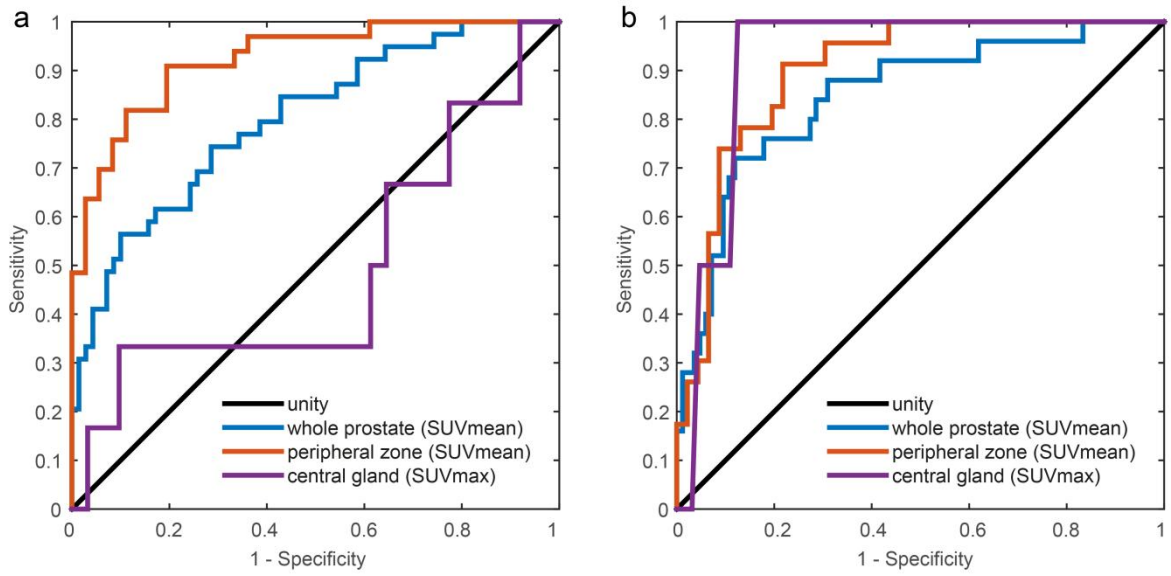

Tables

Table 1 Specifications of the complete PET/MR imaging protocol. MRI sequences not relevant to this study in are coloured gray

Name[a]	Bed position[b]	Orientation	TR/TE (ms)[c]	Matrix	No. slices	Resolution (mm)	
						in-plane	slice
T2W TSE	BP1	Sagittal	5590/100	320 x 320	19	0.6 x 0.6	3.0
T2W TSE	BP1	Transverse	6840/104	384 x 384	23	0.5 x 0.5	3.0
T2W TSE	BP1	Coronal	5470/101	320 x 320	19	0.6 x 0.6	3.0
SS-EPI (DWI)	BP1	Transverse	6100/67	96 x 102	23	2.5 x 2.5	3.0
----- *Change table position; injection of [^{18}F]Fluciclovine* -----							
PET	BP2	Transverse	N.A.	344 x 344	127	2.1 x 2.1	2.0
T1W TSE	BP2	Coronal	815/10	384 x 384	50	0.9 x 0.9	3.3
SS-EPI (DWI)	BP2	Coronal	10400/67	98 x 100	40	2.6 x 2.6	4.4
T2W SPACE	BP2	Coronal (3D)	1500/82	320 x 320	144	1.0 x 1.0	1.1
----- *Change table position* -----							
PET	BP1	Transverse	N.A.	344 x 344	127	2.1 x 2.1	2.0
PRESS (MRSI)	BP1	Transverse (3D)	750/145	12 x 12	10	7.0 x 7.0	7.0
T1W VIBE (DCE)	BP1	Transverse (3D)	4.2/0.97	128 x 128	26	1.8 x 1.8	3.0

[a] T2W: T2-weighted; TSE: Turbo Spin Echo; SS-EPI: Single Shot Echo Planar Imaging; DWI: Diffusion Weighted Imaging; T1W: T1-weighted; SPACE: Sampling Perfection with Application-optimized Contrasts using different flip angle Evolution; PRESS: Point RESolved Spectroscopy; MRSI: MR Spectroscopy Imaging; VIBE: Volume Interpolated Gradient Echo; DCE: Dynamic Contrast Enhanced; [b] BP1 = bed position 1; BP2 = bed position 2; [c] TR = Repetition Time; TE = Echo Time;

Table 2 Statistical analysis at the organ level, for the three candidate windows (W1-3). SUV_{mean} and SUV_{max} given as median (range). N represents the number of VOIs. Bold p-values indicate statistically significant different from prostate

VOI	W1	W2	W3
Prostate			
N	28	28	28
SUV_{mean}	2.6 (1.6-3.5)	2.3 (1.4-2.9)	2.1 (1.5-2.7)
SUV_{max}	6.0 (4.4-10.6)	5.0 (3.2-8.4)	4.7 (2.8-8.9)
Bladder			
N	28	28	28
SUV_{mean}	1.0 (0.5-2.1)	2.6 (1.0-9.4)	3.3 (1.3-12.5)
p-value	**<0.001**	0.176	**<0.001**
SUV_{max}	2.9 (1.7-20.4)	5.7 (1.7-43.7)	6.4 (2.3-39.9)
p-value	**<0.001**	0.712	0.058
Blood pool			
N	28	28	28
SUV_{mean}	1.0 (0.7-1.4)	0.9 (0.6-1.1)	0.8 (0.6-1.1)
p-value	**<0.001**	**<0.001**	**<0.001**
SUV_{max}	1.4 (1.0-2.0)	1.1 (0.8-1.6)	1.2 (0.8-1.8)
p-value	**<0.001**	**<0.001**	**<0.001**

Table 3 Statistical analysis at the sub-glandular level, for the three candidate windows (W1-3). SUV_{mean} and SUV_{max} given as median (range). N represents the number of VOIs. Bold p-values indicate statistically significant different from tumour

	Whole gland			**Peripheral zone**			**Central gland**		
	W1	**W2**	**W3**	**W1**	**W2**	**W3**	**W1**	**W2**	**W3**
Tumour									
N	39	39	39	33	33	33	6	6	6
SUV_{mean}	3.1 (1.5-5.1)	2.7 (1.3-4.1)	2.5 (1.6-3.7)	3.1 (1.5-5.1)	2.8 (1.8-4.1)	2.6 (1.7-3.7)	2.1 (1.8-3.3)	1.9 (1.3-3.4)	2.0 (1.6-3.3)
SUV_{max}	5.5 (2.6-10.6)	4.5 (2.7-8.4)	3.7 (2.3-8.9)	5.7 (2.6-10.6)	4.7 (2.9-8.4)	3.7 (2.5-8.9)	4.0 (3.1-6.1)	3.5 (2.7-5.6)	3.0 (2.3-5.4)
BPH									
N	36	36	36	4	4	4	32	32	32
SUV_{mean}	3.1 (1.1-4.5)	2.4 (1.0-3.5)	2.0 (1.0-3.1)	1.3 (1.1-2.3)	1.3 (1.0-1.9)	1.4 (1.0-1.6)	3.1 (1.6-4.5)	2.4 (1.3-3.5)	2.1 (1.4-3.1)
p-value	0.771	**0.006**	**<0.001**	**0.003**	**0.003**	**0.003**	0.093	0.143	0.809
SUV_{max}	4.5 (1.9-7.9)	3.5 (1.8-5.9)	2.9 (1.7-5.2)	2.4 (1.9-4.3)	2.3 (2.0-2.6)	2.1 (1.9-2.4)	4.8 (2.1-7.9)	3.6 (1.8-5.9)	2.9 (1.7-5.2)
p-value	**0.026**	**<0.001**	**<0.001**	**0.008**	**0.006**	**0.006**	0.433	0.984	0.707
Inflammation									
N	6	6	6	4	4	4	2	2	2
SUV_{mean}	2.2 (1.8-3.2)	2.0 (1.8-2.5)	1.7 (1.4-2.0)	1.9 (1.8-3.2)	2.0 (1.8-2.5)	1.7 (1.4-2.0)	2.4 (2.3-2.4)	2.0 (2.0-2.0)	1.7 (1.6-1.8)
p-value	**0.021**	**0.007**	**<0.001**	**0.03**	**0.006**	**0.003**	n.a.	n.a.	n.a.
SUV_{max}	3.3 (2.7-4.9)	2.6 (2.5-4.1)	2.3 (2.1-2.8)	3.4 (2.7-4.9)	2.8 (2.5-4.1)	2.3 (2.1-2.8)	3.3 (3.2-3.4)	2.5 (2.5-2.6)	2.4 (2.1-2.7)
p-value	**0.005**	**0.002**	**0.001**	**0.013**	**0.010**	**0.007**	n.a.	n.a.	n.a.
Healthy									
N	28	28	28	28	28	28	28	28	28
SUV_{mean}	2.5 (1.4-3.5)	2.1 (1.5-2.8)	2.0 (1.5-2.6)	2.1 (1.1-3.7)	2.0 (1.3-3.1)	1.8 (1.3-2.6)	2.6 (1.9-3.5)	2.2 (1.5-2.8)	2.0 (1.5-2.6)
p-value	**<0.001**	**<0.001**	**<0.001**	**<0.001**	**<0.001**	**<0.001**	0.238	0.297	1.000
SUV_{max}	5.4 (3.5-9.7)	4.1 (3.1-7.4)	3.7 (2.7-7.0)	4.6 (2.5-9.7)	3.9 (2.8-7.4)	3.4 (2.4-6.0)	5.1 (3.5-6.5)	4.0 (3.1-6.3)	3.7 (2.5-7.0)
p-value	0.894	0.401	0.924	**0.007**	**0.011**	**0.021**	0.404	0.433	0.433

Table 4 Statistical analysis at the tumour level, for the three candidate windows (W1-3). SUV_{mean} and SUV_{max} given as median (range). N represents the number of VOIs. Bold p-values indicate statistically significant different from high-grade tumour

TUMOURS	Whole gland			Peripheral zone			Central gland		
	W1	**W2**	**W3**	**W1**	**W2**	**W3**	**W1**	**W2**	**W3**
High-grade									
N	25	25	25	23	23	23	2	2	2
SUV_{mean}	3.1 (1.9-5.1)	2.8 (1.3-4.1)	2.6 (1.6-3.7)	3.1 (2.3-5.1)	2.8 (1.8-4.1)	2.6 (1.9-3.7)	2.6 (1.9-3.3)	2.4 (1.3-3.4)	2.5 (1.6-3.3)
SUV_{max}	5.9 (3.4-10.6)	4.9 (3.4-8.4)	4.7 (2.8-8.9)	5.9 (3.4-10.6)	4.9 (3.4-8.4)	4.6 (2.8-8.9)	5.7 (5.2-6.1)	5.1 (4.6-5.6)	5.0 (4.7-5.4)
Low/interme-diate-grade									
N	14	14	14	10	10	10	4	4	4
SUV_{mean}	2.8 (1.5-4.0)	2.4 (1.8-3.6)	2.1 (1.7-3.3)	3.2 (1.5-4.0)	2.7 (2.0-3.6)	2.3 (1.7-3.3)	2.1 (1.8-2.7)	1.9 (1.8-2.1)	2.0 (1.9-2.1)
p-value	0.173	0.108	**0.040**	0.769	0.667	0.265	n.a.	n.a.	n.a.
SUV_{max}	4.1 (2.6-6.2)	3.6 (2.7-5.9)	3.0 (2.3-5.0)	5.3 (2.6-6.2)	4.5 (2.9-5.9)	3.2 (2.5-5.0)	3.6 (3.1-4.3)	3.1 (2.7-3.5)	2.9 (2.3-3.0)
p-value	**0.005**	**0.005**	**0.001**	0.065	0.088	**0.028**	n.a.	n.a.	n.a.

Electronic Supplementary Material

ESM 1 ROC curve analysis, for the three candidate windows (W1-3). Data is presented as percent sensitivity/specificity/area under the curve. Bold values indicate the combination of window and SUV-parameter with area under the curve statistically significant different from 50%

	Whole gland			**Peripheral zone**			**Central gland**		
	W1	**W2**	**W3**	**W1**	**W2**	**W3**	**W1**	**W2**	**W3**
Tumour vs. benign tissue									
SUV_{mean}	**72/56/65%**	**72/81/76%**	**74/71/80%**	**88/86/89%**	**88/89/94%**	**82/89/92%**	17/81/24%	17/98/28%	83/31/48%
SUV_{max}	**62/60/62%**	**67/73/72%**	**54/73/68%**	**79/72/77%**	**73/75/76%**	**85/56/74%**	33/60/33%	33/85/44%	33/90/49%
High-grade tumour vs. all other tissue									
SUV_{mean}	**68/64/70%**	**84/76/81%**	**76/82/85%**	**96/74/83%**	**87/83/87%**	**91/78/90%**	50/80/42%	50/97/49%	50/98/55%
SUV_{max}	**76/61/75%**	**80/70/81%**	**72/74/81%**	**83/70/81%**	**78/67/78%**	**78/67/81%**	100/58/73%	**100/83/90%**	**100/88/92%**

ESM 2 Median (line + marker) and median absolute deviation (shaded area) of the dynamic SUV_{mean} curves in lymph node VOIs and blood pool VOIs, overlaid with the position of the early (W1) and late candidate windows (W2 and W3). The data represent the 70% isocontour SUVs of four lymph nodes metastases that were clearly visible on PET, and their corresponding blood pool SUVs. The median absolute deviation is calculated as the median value of the absolute differences between the individual SUVs and their median value